BIOCHEMICAL PHARMACOLOGY 75 (2008) 761–772

available at www.sciencedirect.com

ScienceDirect

journal homepage: www.elsevier.com/locate/biochempharm

Differential regulation of cell death in head and neck cell carcinoma through alteration of cholesterol levels in lipid rafts microdomains

Clara Bionda [a,b,c], *Anne Athias* [f], *Delphine Poncet* [e], *Gersende Alphonse* [a,b,c,d], *Amel Guezguez* [a,b,c], *Philippe Gambert* [f], *Claire Rodriguez-Lafrasse* [a,b,c], *Dominique Ardail* [a,b,c,*]

[a] *EA 3738, Laboratoire de Radiobiologie Cellulaire et Moléculaire, Faculté de Médecine Lyon-sud, Lyon F-69921, France*
[b] *Université de Lyon, Lyon F-69003, France*
[c] *Université Lyon 1, France*
[d] *Hospices Civils de Lyon, Service de Radiothérapie, Centre Hospitalier Lyon-sud, Lyon F-69495, France*
[e] *Laboratoire de Biologie des Tumeurs, Centre Hospitalier Lyon-sud, Lyon F-69495, France*
[f] *Unité INSERM U498, Dijon F-21000, France*

ARTICLE INFO

Article history:
Received 1 August 2007
Accepted 1 October 2007

Keywords:
Methyl-beta-cyclodextrine
Lipid rafts
Cholesterol
Apoptosis
Head and neck squamous cell carcinoma
Fas
EGF receptor

ABSTRACT

Lipid rafts are cholesterol-enriched microdomains in the plasma membrane. They act as molecular platforms that spatially organize membrane receptor molecules and are involved in the transduction of various signaling pathways. We recently reported that in the radiosensitive squamous cell carcinoma SCC61 line, γ-irradiation results in a rearrangement of the plasma membrane rafts and signaling platforms leading to radiation-induced apoptosis in a ceramide-dependent pathway. By contrast, this reorganization was found to be defective in the radioresistant counterpart cell line, SQ20B. As the cholesterol content of lipid rafts is two times higher in SQ20B compared with SCC61 cells, we investigated the modulation of these microdomains using methyl-beta-cyclodextrin (MβCDX), a widely used cholesterol-depleting agent, in order to disrupt raft organization in both cells. Here, we report that MβCDX treatment resulted in the triggering of apoptosis in SCC61 cells involving mitochondrial events and associated with the clustering of Fas, the formation of Fas–FADD complexes and the cleavage of procaspase 8. The ligand-independent activation of this death receptor was totally absent in SQ20B cells, which remained resistant to MβCDX-triggered apoptosis. However, treatment of SQ20B with MβCDX resulted in a ligand-independent activation of the epidermal growth factor receptor (EGFR) survival pathway, as evidenced by an increased tyrosine phosphorylation of EGFR. Taken altogether, our results indicate that lipid raft integrity is intimately involved in the triggering of apoptotic cell death and/or survival pathways in head and neck carcinoma cells.

* *Corresponding author at*: Laboratoire de Radiobiologie Cellulaire et Moléculaire, UFR Médicale Lyon-sud, BP 12, 69 921 Oullins cedex, France. Tel.: +33 4 26235955; fax: +33 4 26235966.
E-mail address: ardail@sante.univ-lyon1.fr (D. Ardail).
0006-2952/$ – see front matter
doi:10.1016/j.bcp.2007.10.004

1. Introduction

Cholesterol is an abundant component of the plasma membrane of eukaryotic cells that plays a pivotal role in the regulation of membrane fluidity, permeability, receptor function and ion channel activity [1–4]. The lateral distribution of cholesterol in the membrane is not uniform and its content is particularly high in raft microdomains that are also enriched in gangliosides and sphingolipids [5,6]. These domains have been reported to act as molecular platforms that spatially organize membrane receptor molecules [3,7]. The association of receptors with lipid rafts often enhances the efficiency of signaling, as has been demonstrated for B and T cell antigen receptors [3,7,8]. Moreover, there is growing evidence that lipid rafts are involved in the signal transduction of various pathways, coupled either with glycosylphosphatydyliositol-anchored proteins or with receptor tyrosine kinases [3,9,10]. A variety of studies have demonstrated that many stimuli such as CD95 (or Fas), CD40, FcγRII, CD20, cisplatin, UV light and gamma radiation (γ-radiation) can induce the formation of membrane platforms, a fundamental process in the initiation of signal transduction (see [11] for review). This reorganization is of crucial importance in the initiation and regulation of inflammatory processes and apoptosis. Thus, redistribution of death receptors such as Fas to cholesterol-enriched lipid domains has been proposed to be an important regulatory step during the activation of the apoptotic death program [12–14]. Numerous studies reported that depletion of cholesterol, which is present at higher concentrations in lipid rafts than in the bulk plasma membrane, can alter the function of a variety of membrane receptors [15], and signaling pathways at the cell surface [16,17]. Methyl-β-cyclodextrin (MβCDX) is a water-soluble cyclic heptasaccharide that binds cholesterol with high specificity and has been widely used to disrupt the integrity of these domains [18–20]. However, the effect of this cholesterol-depleting agent on the triggering of the apoptotic death process is still a matter of debate. In HaCaT cells, Gniadecki [21] found that raft disruption resulted in a ligand-independent Fas activation, thereby triggering the cleavage of pro-caspase-8. By contrast, Hueber et al. [22] reported that in mouse thymocytes and L12.10-FasT cells, raft disruption abolishes the Fas-mediated formation of the death-inducing signaling complex (DISC) thus inhibiting Fas-induced cell death. Additional experiments demonstrated that raft disruption by MβCDX prevents apoptotic cell death induced by various stimuli including UVB irradiation [23], CD95 stimulation [12,24–26] or various antitumor agents [27,28]. However, MβCDX treatment causes cell death in unstimulated acute myeloid leukaemia cells [29], but not in the lymphoma cell line SW49 [27].

Our group previously demonstrated that SCC61, a model of a human squamous cell carcinoma line, can undergo apoptosis after Fas induction [30] and after γ-irradiation [31], while this apoptotic pathway is defective in the resistant counterpart SQ20B cell line after these two stimuli. Moreover, we recently reported [32], that γ-irradiation of the radiosensitive SCC61 cells resulted in the coalescence of pre-existing lipid rafts to larger domains. This recruitment was immediately followed by the production of ceramide in these domains, leading to the triggering of apoptosis in a ceramide-dependent pathway, 24 h after irradiation of SCC61 cells [31]. By contrast, the rearrangement of the plasma membrane rafts and ceramide release were found to be defective in the radioresistant SQ20B cell line [32], a result that could partially explain the defect of the apoptotic response following either Fas or γ-radiation. Based on these considerations, it was therefore of great interest to determine if lipid rafts are intimately involved in the control of apoptotic death in squamous cell carcinoma SCC61 and SQ20B. As the lipid composition of rafts could directly affect the physical properties of the membrane, such as thickness, fluidity or lateral domain formation [2,33], we investigated whether the composition of lipid rafts in these two cell lines and its modulation by MβCDX could play a significant role in the triggering of the apoptotic pathway.

2. Materials and methods

2.1. Antibodies and reagents

The following antibodies were used: rabbit anti-Fas (clone C-20), mouse anti-Fas coupled to agarose (clone B-10), rabbit anti-FADD (clone H-181), rabbit anti-EGFR (clone 1005), rabbit anti-phosphorylated EGFR (Tyr 1173) and horseradish peroxidase conjugated to secondary antibodies against rabbit and mouse antibodies were purchased from Santa Cruz Biotechnology (Santa Cruz, CA), mouse anti-caspase 8 (clone 5F7) from Euromedex (Mudolsheim, France), mouse monoclonal anti-GAPDH was obtained from Biodesign. FITC-labeled goat α-mouse IgG and FITC labeled goat α-rabbit IgG were purchased from Jackson ImmunoResearch Laboratories (West Grove, PA). Methyl-beta-cyclodextrine (MβCDX) and pOH phenyl acetic acid were purchased from Sigma–Aldrich (St Louis, MO).

2.2. Cell culture and irradiation

The human head and neck squamous cell carcinoma lines (HNSCC), SQ20B and SCC61 were obtained from J.B. Little (Laboratory Department of Cancer Biology, Harvard School of Public Health, Boston, USA) [34], cultured in Dulbecco's Modified Eagle's Medium (DMEM) (Gibco, Invitrogen), at 37 °C in 5% CO_2. The culture medium was supplemented with 10% (v/v) heat inactivated fetal calf serum, 100 units/ml penicillin and 100 μg/ml streptomycin, 0.4 μg/ml hydrocortisone and 0.1% fungizone (all from Gibco, Invitrogen). SQ20B and SCC61 cells were irradiated with X rays at room temperature for 4.16 min at 2.4 Gy/min, corresponding to 10 Gy, with the Saturn 42 irradiator (Varian Medical Systems, Palo Alto, CA).

2.3. Isolation of rafts membrane

Membrane rafts were isolated from cells as previously described [35]. For each preparation, 10×10^7 cells were washed twice with PBS. Cells were scraped and pelleted by centrifugation, resuspended in 1 ml of ice-cold Tris Buffer Saline (TBS) (150 mM NaCl, 5 mM EGTA, 10 mM Tris-HCl, pH 7.5), containing 1% (w/v) Triton X100 and protease inhibitors (protease inhibitors cocktail tablets, EDTA free, Roche, France). The sample was homogenized in a Dounce (20 times), adjusted

to 40% (w/v) sucrose in TBS and loaded under a 5–30% (w/v) linear sucrose gradient in TBS. Following centrifugation in a SW55Ti Rotor at 34000 rpm for 20 h at 4 °C, six fractions of 900 μl were collected from the top and stored at −80 °C. Protein concentrations were measured by the bicinchoninic acid (BCA) method using bovine serum albumin as standard. As control and described previously [32], caveolin-1 was used as a marker of caveolae, whereas GAPDH was found in soluble membrane fractions.

2.4. Quantitative analysis of fatty acid, cholesterol, oxysterol and phospholipids from SQ20B and SCC61 rafts and non-rafts fraction

2.4.1. Sterols, phospholipids and fatty acids analysis from raft and non-rafts fractions

Lipids of 300 μl of sample were extracted by chloroform/methanol (3:2, v/v) with 50 mg/l of BHT. Epicoprostanol (*m/z* 370), 19 hydroxycholesterol (*m/z* 353), dimyristoylphosphatidylcholine (*m/z* 678), lauroylsphingomyéline (*m/z* 647) and lauroyllysophosphatidylcholine (*m/z* 440) were used as internal standards for cholesterol, oxysterols, phosphatidylcholine, sphingomyelin and lysophosphatidylcholine, respectively.

2.4.2. Phospholipids analysis

An aliquot of the chloroformic phase was evaporated and 100 μl of chloroform/methanol (4:1, v/v) was added for quantitative LC/MS. Phospholipids analysis was performed on a Hypersil Si 2 × 200 mm column (Agilent Technologies) with a binary gradient of solvent A (5 mM ammonium acetate in chloroform/methanol (4:1, v/v) and solvent B (5 mM ammonium acetate in chloroform/methanol/water 6:3.4:0.5, v/v/v) [36]. Elution was performed at a flow rate of 0.3 ml/min. Positive ESI-MS was performed on a MSD 1100 single quadrupole Mass Spectrometer (Agilent Technologies). The orifice voltage was set at 120 V, the capillary voltage at 3.5 kV, the drying gas flow at 8 l/mn and scan range from *m/z* 400 to 950.

2.4.3. Cholesterol and oxysterols analysis

Another aliquot of the chloroformic phase was evaporated, 60 μl of KOH 10 M and 1 ml of methanol were added and tubes were incubated during 2 h at 37 °C. After incubation, 2 ml of chloroform and 1ml of water were added, tubes were shaken, centrifuged and the chloroformic phase was evaporated. 100 μl of a mixture of bis(trimethylsilyl)trifluoroacetamide/trimethylchlorosilane 4:1 (v/v) (Acros organics) [37] was added, tubes were incubated 1 h at 80 °C, evaporated and 100 μl of hexane was added. Trimethylsilylethers of sterols analysis was performed by GC/MS in a 6890 gas chromatograph coupled with a 5973 Mass Detector (Agilent Technologies). The column was a HP-5MS 30 m × 0.25 mm (Agilent Technologies), helium was used as the carrier gas. The GLC operating conditions were as follows: injector temperature was 250 °C and oven temperature was programmed, after injection, at a rate of 10 °C/min from 180 to 260 °C then at a rate of 1 °C/min to 280 °C. The MSD operating conditions for EI-MS were: source temperature 230 °C, ionising voltage 70 eV. The mass spectrometer was operated in the selected ion monitoring mode. The ions used for analysis (*m/z*) were as follows: cholesterol: 368, epicoprostanol: 370, 7λ and 7β-hydroxy-cholesterol: 456 and 7-ketocholesterol: 472.

Concentrations of phospholipids and sterols were determined from the ratio of the peak area corresponding to one given molecule to the peak area corresponding to the internal standard. Levels were determined by comparison of this ratio with a standard curve of known amounts of cholesterol, oxysterols and different species of phospholipids.

2.5. Treatment with MβCDX and quantification of cholesterol

Cells were switched to the serum-free DMEM before incubation with the indicated concentrations of MβCDX dissolved in DMEM at 37 °C. For experiments with irradiation, MβCDX was added 1 h before irradiation. Quantification of total cell content of cholesterol was measured as previously reported [38]. Cells were scraped and extracted for 4 h with chloroform/methanol (1:1, v/v). After centrifugation, the organic phase was collected and dried under nitrogen for cholesterol quantification; the pellet was dissolved in 1 ml of NaOH for protein determination by the bicinchoninic acid method. For cholesterol determination, 1 ml of solution (0.1 M K_2HPO_4/KH_2PO_4 buffer, pH 7.4, 0.5%Triton X100 (w/v), 0.4% pOH phenyl acetic acid (w/v), 20 mM Na cholate, 0.25% 45 U cholesterol oxidase (w/v), 10 U/ml peroxydase, 0.1% 55 U cholesterol esterase (w/v)) was added on dried sample and incubated 30 min at 37 °C. The fluorescence intensity was measured on the RF 5301 PC spectrofluorophotometer (Shimadzu), with λ excitation at 320 nm and λ emission at 402 nm. Treatment of SQ20B and SCC61 cells with 1% MβCDX for 1 h led to approximately a 60–70% decrease in the cellular cholesterol level.

2.6. Clonogenic assay

SCC61 and SQ20B cells were seeded on 25 cm^2 plastic flask (Corning, Int, NY, USA) and allowed to adhere overnight. Next morning, cells were treated with MβCDX, at different concentration (0.1–1%) and during different time (15 min to 8 h). Then cells were cultured in DMEM/FCS for 12 days and fixed with ethanol 30 min and stained 1 h with crystal violet (1%, w/v). Visible colonies larger than 2 mm in diameter were counted manually.

2.7. BrdU labeling for necrosis quantification

Necrotic and apoptotic cells were quantified using the Cellular DNA fragmentation ELISA kit (Roche Diagnostics, Penzberg, Germany). Briefly, SQ20B and SCC61 cells were incubated overnight with 10 μM bromodeoxyuridine (BrdU). After serum depletion and treatment with 1% MβCDX for 1 h, the measurement of apoptotic cell death was performed using the BrdU assay. The BrdU-labeled DNA was detected and quantified using a monoclonal anti-BrdU-antibody–peroxidase conjugate followed by photometric measurement at 450 nm (reference wavelength 690 nm).

2.8. Flow cytometry

For cell-cycle analysis, cells were pelleted and fixed in ice-cold 70% ethanol and stored at −20 °C for at least 24 h before labeling. After washing with PBS and subsequent centrifuga-

tion, cells were re-suspended in a solution containing 0.5 ml propidium iodide (500 μg/ml), 0.25 ml RNAse (1 mg/ml) and 0.25 ml PBS and incubated for 15 min in the dark at room temperature before flow-cytometric analysis on a Coulter Epics XL.MLC (Beckman Coulter, Villepinte, France). Hypodiploid (apoptotic) cells appear in the cell-cycle distribution as cells with DNA content less than G1.

The estimation of reactive oxygen species (*ROS*) was quantified after incubation of cells with 4 μM hydroethidine (HE) in the dark for 20 min, which permeates the cell membrane and can be oxidized into red fluorescent ethidium bromide (Eth) in the presence of superoxide anion. By flow cytometry, 10,000 events for each sample were analyzed for red fluorescence (FL2).

To measure the mitochondrial membrane potential ($\Delta\psi_m$), cells were incubated in the dark for 20 min with 5 μg/ml JC-1. This cyanine dye has the property of accumulating in the mitochondrial membrane potential and to form J-aggregates with a characteristic absorption and emission spectra. After analysis of 10,000 events by flow cytometry, the increase of green fluorescence (FL1), corresponding to monomer formation in the dye, was taken as a measure of decreased $\Delta\psi_{m.}$

2.9. Western immunoblotting

Cell pellets were lysed in 50 mM Tris buffer (pH 8.0), 150 mM NaCl, 1% Triton X-100 and protease inhibitors (protease inhibitor cocktail tablets, EDTA-free, Roche, Meylan, France), for 1 h at 4 °C. Lysates were centrifuged for 20 min at 15,000 × *g* and an aliquot of the supernatant was mixed with denaturation buffer (125 mM Tris–HCl, pH 6.8, 4% SDS, 5% β mercaptoethanol, 0.05% bromophenol blue) for 5 min at 100 °C. Proteins were separated on 12% polyacrylamide gel by electrophoresis, transferred to a nitrocellulose membrane (Bio-Rad) and blocked with 5% nonfat milk in TBS–Tween 20 (0.05%) at room temperature for 1 h. Blots were incubated then with primary antibody for overnight: rabbit anti-FAS (dilution at 1/300° in TBS–Tween 0.05%–fat milk 5%), rabbit anti-FADD (dilution at 1/300° in TBS–Tween 0.2%–non-fat milk 5%), rabbit anti-EGFR (dilution at 1/300° in TBS–Tween 0.05%–fat milk 5%), rabbit anti-phosphorylated EGFR (Tyr 1173, dilution at 1/200° in PBS–Tween 0.5%–fat milk 5%), mouse anti-caspase 8 (dilution at 1/1000° in PBS–Tween 0.05%–fat milk 3%) or mouse anti-GAPDH (dilution at 1/15,000° in TBS–Tween 0.05%–fat milk 5%). Membranes were washed before addition of anti-rabbit or anti-mouse IgG secondary antibodies and incubated for 1 h at room temperature. Proteins were visualized using an ECL kit (Pierce, Amersham Bioscience) and exposed to a Biomax MR film (Eastman Kodak).

2.10. Immunoprecipitation

Fas immunoprecipitation: Cells were lysed in ice-cold RIPA buffer (Tris–HCl 50 mM, pH 7.2, NaCl 150 mM, SDS 0.1%, NP40 1%, deoxycholate 0.5% and Roche's complete protease inhibitor) and cell lysates (600 μl) were immunoprecipitated overnight at 4 °C with a mouse monoclonal anti-Fas antibody coupled to agarose. Immunocomplexes were resolved by SDS-PAGE, blotted on PVDF membranes, and probed with specific antibodies. After incubation with a secondary antibody, proteins were detected by ECL chemiluminescence.

2.11. Confocal microscopy

Cells were cultured on 24 mm × 24 mm coverslips in 24-well microtiter plates, one night before the experiments. Cells were treated or not with MβCDX, fixed for 10 min in 4% PFA (w/v) in PBS and washed in PBS containing 3% BSA (w/v) and 10 mM Hepes (PBS-BSA-Hepes). Cells were then incubated for 45 min with a mouse polyclonal anti-FAS and a rabbit anti-FADD (1:100 dilution) or with rabbit anti-phosphorylated EGFR (dilution at 1:100). Cells were then washed and stained for 45 min with FITC-labeled goat anti-rabbit or anti-mouse (1:200 dilution). After a final wash, cells were mounted on glass cover slips with Fluoprep mounting medium. Control staining was performed with secondary antibodies alone. Slides were examined at the Quantimetry Platform of Rockefeller (Pr Tourneur, Lyon, France) with a Leica TCS SP2 Confocal microscope (Germany) using a Plan-Apochromat 63× objective (1.4 oil). An argon laser at 488 nm was used to excite FITC (emission 515–540 nm) and a helium–neon laser was filtered at 633 nm or 550 nm to excite AlexaFluor 647 and AlexaFluor 488 (emission 680 nm and 570 nm), as regulated by SP2 software (Leica). For co-localization, images were recorded in multitracking mode and images were obtained using Image J software (Leica).

2.12. Statistical analysis

All data were analyzed and presented as mean ± S.D. ($n < 10$). The significance of differences between populations of data were assessed according to the Student's two-tailed *t*-test with a level of significance of at least $p < 0.05$ (alpha conventionally equal to 0.05).

3. Results

3.1. Comparative study of lipids in raft and non-raft fractions extracted from SQ20B and SCC61 cells

Our previous results showed a defective rearrangement after ionizing radiation of plasma membrane raft microdomains in radioresistant SQ20B cells, compared with radiosensitive SCC61 cells [32]. We therefore investigated the lipid composition of both nondetergent resistant-membrane and detergent resistant-membrane fractions in the two cell lines. Lipids were extracted and major lipid components of raft fractions (sphingomyelin, phosphatidylcholine, lysophosphatidylcholine, cholesterol and oxidized cholesterol) analyzed by LC/MS and GC/MS. Although sphingomyelin and cholesterol were, as expected, enriched in the detergent resistant-membrane fractions of both cell lines, the results reported in Table 1 indicate that the major difference in lipid raft content was in cholesterol, which was twice as high (2.678 ± 0.313 nmol/mg of protein) in SQ20B rafts as in rafts from SCC61 cells (1.367 ± 0.026 nmol/mg of protein, $p < 0.01$). By contrast, oxysterols were found to be higher in the radiosensitive SCC61 cell line compared with SQ20B. No other major differences between these two cell lines in the lipid composition of rafts were found.

Table 1 – Lipid composition of lipids in rafts and non-rafts fraction isolated from SCC61 and SQ20B cells by density gradient centrifugation

	SCC61 rafts (nmol/mg prot.)	SQ20B rafts (nmol/mg prot.)	SCC61 non-rafts (nmol/mg prot.)	SQ20B non-rafts (nmol/mg prot.)
Sphingomyelin	0.210 ± 0.0001	0.260 ± 0.036	0.007 ± 0.0001	0.003 ± 0.0001
Phosphatidylcholine	0.636 ± 0.052	0.857 ± 0.127	0.001 ± 0.0001	0.015 ± 0.0001
Lysophosphatidylcholine	0.001 ± 0.0001	0.002 ± 0.003	0.002 ± 0.0001	0.03 ± 0.0001
Cholesterol	1.367 ± 0.026	2.678 ± 0.313	0.152 ± 0.005	0.224 ± 0.008
7λ OH cholesterol ($\times 10^{-3}$)	0.550 ± 0.046	0.068 ± 0.006	0.105 ± 0.009	0.007 ± 0.0001
7β OH cholesterol ($\times 10^{-3}$)	0.338 ± 0.014	0.126 ± 0.013	0.098 ± 0.005	0.016 ± 0.001
7-Keto cholesterol ($\times 10^{-3}$)	1.061 ± 0.212	0.407 ± 0.057	0.125 ± 0.03	0.041 ± 0.001

Lipids from rafts and non-rafts fractions isolated from SCC61 and SQ20B cells were analyzed by LC/MS for phospholipids studies and GC/MS for sterols analysis, as detailed in Section 2. The concentration of each class of lipids was determined from the ratio of the peak area corresponding to a given molecule to the peak area corresponding to the internal standard. Quantitation was determined by comparison of this ratio with a standard curve of known amounts of different species of phospholipids, cholesterol and oxysterols, reported to mg of protein content, respectively, in rafts or non-rafts fractions (nmol/mg of proteins). The data represent the mean ± S.D. for two determinations.

3.2. MβCDX induces cell death in cultured SCC61 and SQ20B cells

In light of the results reported above, we next investigated the effects in our two cell lines of the cholesterol-depleting agent, MβCDX, used for lipid raft disruption. Cells were starved in serum-free Dulbecco's minimal essential medium for 12 h before treatment with MβCDX in order to avoid receptor activation by growth factors present in fetal calf serum. In the initial series of experiments, we checked for the influence on cultured SQ20B and SCC61 cells of MβCDX concentration and incubation time. The cell survival curves obtained after the clonogenic assay show that the treatment with MβCDX resulted in a time- and concentration-dependent reduction in cell number (Fig. 1), which seemed to be more marked in SCC61 cells than in SQ20B cells. We found that less than 25% of SCC61 cells survived after a 1 h treatment with 1% MβCDX, whereas about 50% of SQ20B cells survived under the same experimental conditions. Thus, SCC61 cells seemed to be more sensitive than SQ20B cells to MβCDX.

As a significant percentage of cell death was measured in the two cells lines in the presence of MβCDX, we next determined the percentage of cells undergoing apoptosis and/or cell-mediated cytotoxicity using the DNA fragmentation ELISA assay. As shown in Fig. 2A, MβCDX was found to trigger apoptosis in SCC61 cells, but not in SQ20B cells even after incubation with higher concentrations of MβCDX (2 and 5%, for 2 and 5 h) (data not shown). By contrast, we found a significant increase of necrotic SQ20B cells, at times up to 60 min (Fig. 2D) after treatment with MβCDX.

3.3. Triggering of apoptosis induced by cholesterol depletion in SCC61 cells

In order to confirm these results, we performed a cell-cycle analysis to evaluate the percentage of sub-G1 cells as an index of apoptosis. As depicted in Fig. 3A, a significant sub-G1 phase occurred 4 h after treatment of SCC61 cells with 1% MβCDX for 1 h that increased to 55%, 48 h after treatment. Similar results were obtained with γ-radiation alone. The combination of both treatments (γ-radiation and MβCDX, 1 h before radiation) resulted in a reinforcement of the MβCDX effect on SCC61 cells of γ-radiation. In SQ20B, few cells (less than 10%) were detected in the sub-G1 phase under the same conditions of treatment (γ-radiation and/or MβCDX) (Fig. 3B).

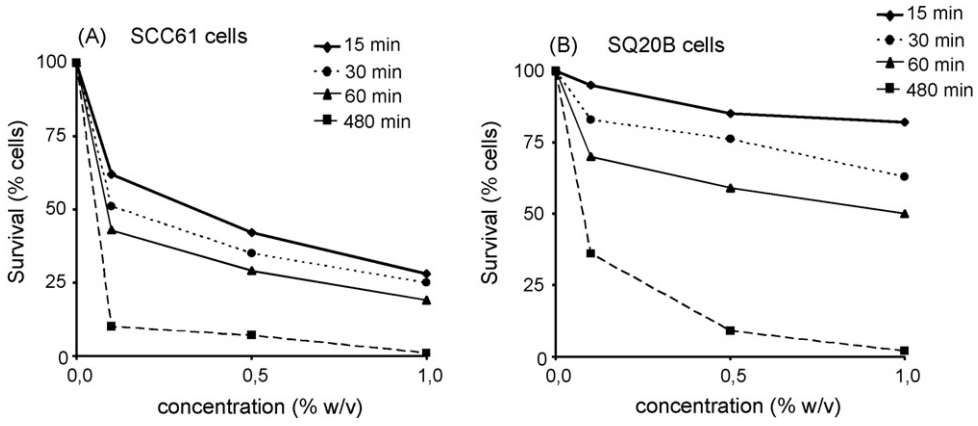

Fig. 1 – Effect of cholesterol depletion by MβCDX on cell viability of SCC61 and SQ20B cells. Serum-starved cells were treated with 0.1, 0.5 or 1% (w/v) MβCDX for 15, 30, 60 or 480 min. Cell viability was measured by the clonogenic assay, after fixation and staining, 12 days post-treatment. Colonies with more than 64 cells were counted and the survival curve was established. Values represent the means of three independent experiments of SCC61 cells (Panel A) and SQ20B (Panel B).

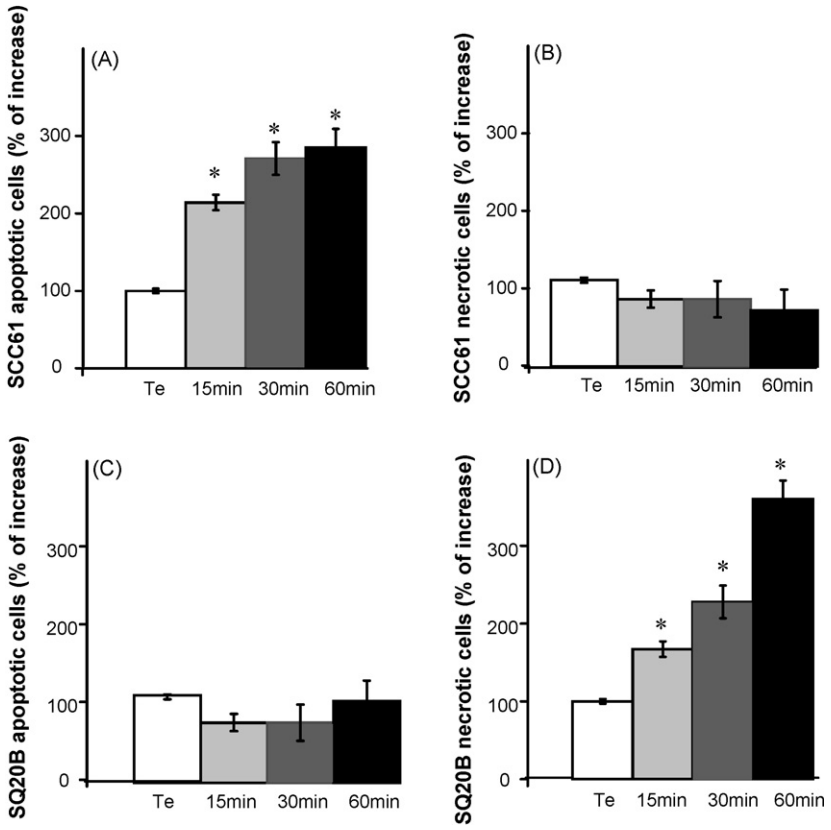

Fig. 2 – Induction of apoptosis in SCC61 cells and necrosis in SQ20B cells by MβCDX. Serum-starved cells were treated with 1% MβCDX for 15, 30 or 60 min and then incubated in complete medium at 37 °C for 48 h. Apoptotic and necrotic cells were quantified using the Cellular DNA fragmentation ELISA Kit (Roche Diagnostics) in a 96-well plate as described in Section 2. Apoptosis (Panels A and C) was measured by detection of BrdU-labeled DNA fragments in the cytoplasm of apoptotic cells whereas necrosis (Panels B and D) was estimated by the detection of BrdU-labeled DNA fragments released into the culture medium. Values represent the mean ± S.D. of two independent experiments performed in triplicate (*$p < 0.05$).

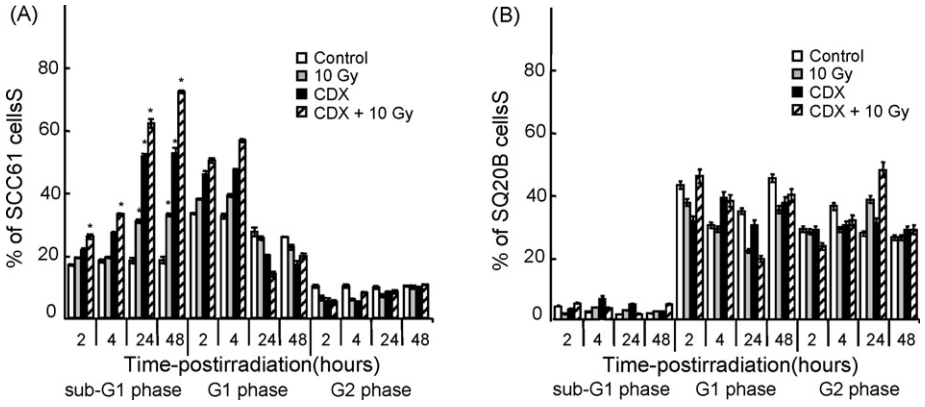

Fig. 3 – Kinetics of cell-cycle progression in SCC61 cells and SQ20B cells after MβCDX treatment. SCC61 (Panel A) and SQ20B (Panel B) cells were irradiated at 10 Gy, treated with MβCDX (1% for 1 h) or treated for 1 h with MβCDX before irradiation at 10 Gy. Thereafter, cells were incubated in a complete culture medium at 37 °C and analyzed 2, 4, 24 and 48 h after treatment. Cell-cycle analysis was performed using flow cytometry and propidium iodide-labelling. Results are expressed as the percentage of cells in each phase according to their DNA content. Values represent the mean ± S.D. of two independent experiments performed in triplicate (*$p < 0.05$).

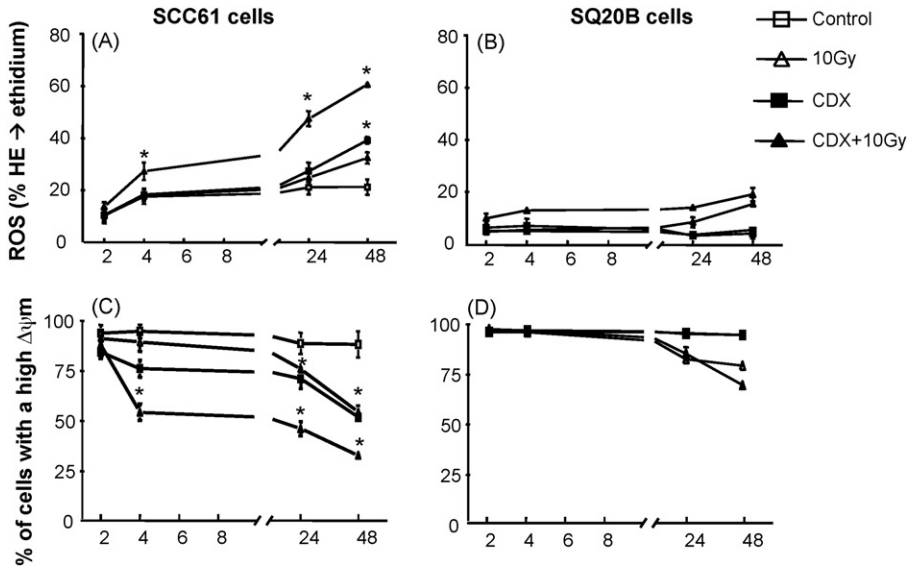

Fig. 4 – Intracellular content of reactive oxygen species (ROS) and mitochondrial membrane potential ($\Delta\psi_m$) measured in reponse to MβCDX alone or in combination with γ irradiation. SCC61 (Panels A and C) and SQ20B (Panels B and D) cells were irradiated at 10 Gy, treated with MβCDX (1% for 1 h) or treated for 1 h with MβCDX before irradiation at 10 Gy. Thereafter, cells were incubated in a complete culture medium at 37 °C and analyzed 2, 4, 24 and 48 h after treatment. ROS generation was assessed by the conversion of hydroethidine (HE) to ethidium and 10,000 events were analyzed by flow-cytometry for red fluorescence (FL2) (Panels A and B). $\Delta\psi_m$ was assessed after JC-1 labelling and 10,000 events were analyzed for green fluorescent (FL1) (Panels C and D). Results are expressed as the percentage of cells with a high $\Delta\psi_m$. Values represent the mean ± S.D. of two independent experiments performed in triplicate (*$p < 0.05$).

Given the crucial role played by mitochondria in the execution of apoptosis, we evaluated the ability of the MβCDX to trigger the mitochondrial events involved in the apoptotic process in SCC61 and SQ20B cells. As shown in Fig. 4A, incubation of SCC61 cells with 1% MβCDX for 1 h induced the generation of reactive oxygen species (ROS), an effect that was already significant at 4 h and increased up to 48 h after treatment. In the same way, we observed an alteration in the mitochondrial permeability transition channel: MβCDX induced a decrease of the number of SCC61 cells with a high mitochondrial membrane potential ($\Delta\psi_m$) 4 h after treatment (75% of the control), which fell to 51%, 48 h after MβCDX treatment (Fig. 4C). As previously observed with flow cytometry, the combination of MβCDX with γ-radiation, strengthened this apoptotic effect, as evidenced by the increase of ROS generation up to 58% and the decrease of cells with a high $\Delta\psi_m$ (27% instead of 75%). In SQ20B cells, MβCDX did not influence ROS generation or $\Delta\psi_m$, discounting any direct effect of this treatment, alone or in combination with γ-radiation on mitochondria (Fig. 4B and D).

3.4. *Cholesterol depletion induces a ligand-independent activation of Fas and apoptosis of SCC61 cells*

We next examined which signaling pathway might be involved in the MβCDX-induced apoptosis of SCC61 cells. As shown in Fig. 5, MβCDX-induced apoptosis was associated with an increased proteolytic cleavage of procaspase 8. As expected, no cleavage of procaspase-8 occured in SQ20B cells treated under the same conditions. This result suggested the involvement of a membrane death receptor, possibly Fas, and of DISC formation in response to MβCDX treatment of SCC61 cells.

Further support for this hypothesis was provided by fluorescence imaging of the Fas receptor (Fig. 6). MβCDX caused a striking aggregation of Fas in the membrane that was perceptible from 5 to 10 min after treatment of SCC61 cells. Fas aggregation seemed to be functional, since receptor clusters colocalized with FADD (Fig. 6B), whereas no colocalization was observed in untreated SCC61 cells or SQ20B cells treated with MβCDX (Fig. 6A and C, respectively).

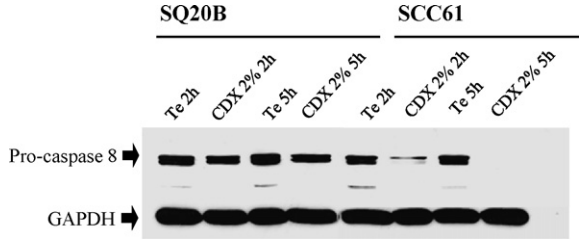

Fig. 5 – Activation of caspase-8 in SCC61 cells after cholesterol depletion with MβCDX. Serum-starved SCC61 and SQ20B cells were treated with MβCDX (2% for 2 or 5 h) and then cells were lysed. Thirty micrograms of proteins from each sample was subjected to immunoblotting analysis using antibodies specific for pro-caspase-8 (54/55 kDa) and GAPDH (37 kDa) (loading control).

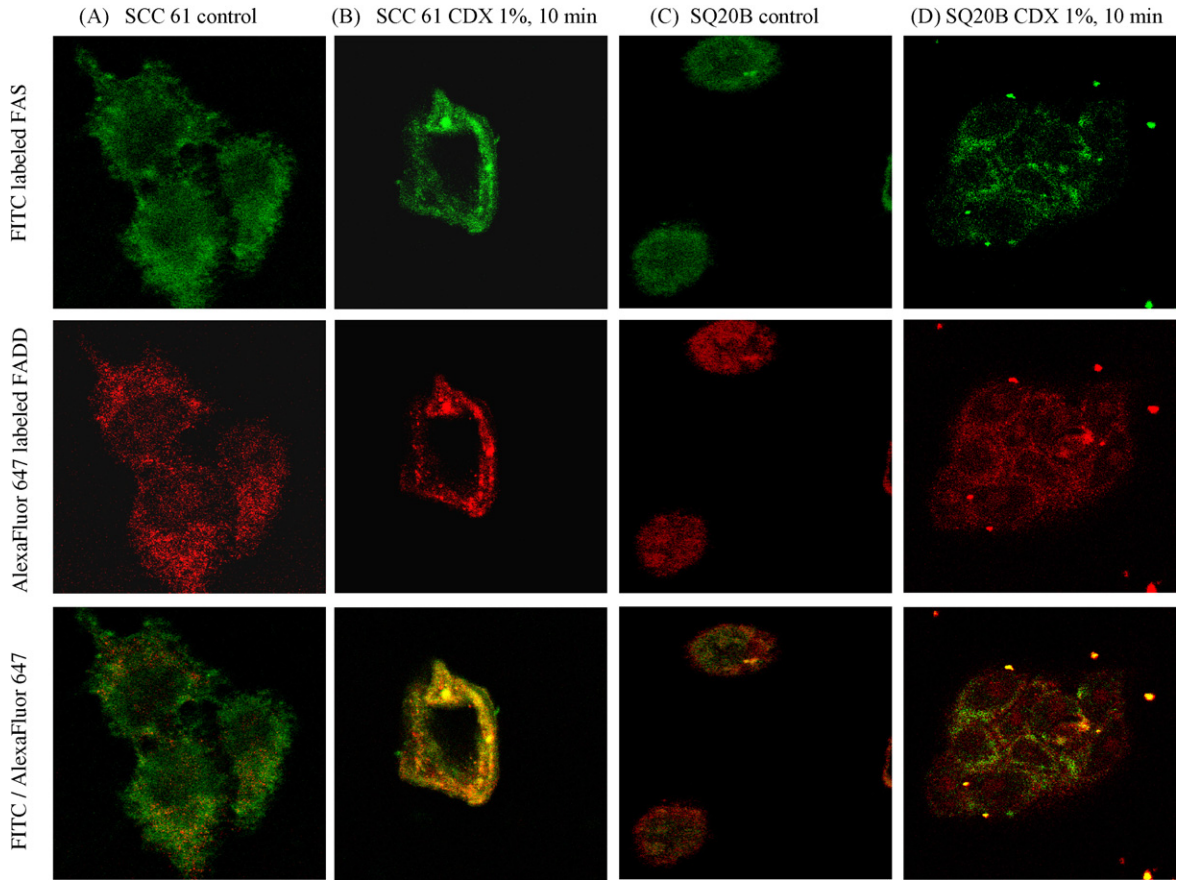

Fig. 6 – Induction of Fas clustering in SCC61 cells after cholesterol depletion with MβCDX. Serum-starved SCC61 and SQ20B cells were treated with MβCDX (1% for 10 min), fixed with 4% PFA and analyzed by confocal microscopy using specific antibodies: anti-Fas coupled to FITC (green emission) and anti-FADD coupled to Alexa 647 (red emission). An overlap between Fas and FADD immunoreactivities suggests formation of Fas–FADD complexes (For interpretation of the references to color in this figure legend, the reader is referred to the web version of the article.).

To further substantiate this claim, we immunoprecipitated the DISC in MβCDX-treated cells using a specific anti-Fas antibody coupled to agarose and separated protein complexes by SDS-polyacrylamide gel electrophoresis. Western blotting revealed increased amounts of FADD and caspase-8 in anti-Fas precipitates of SCC61 cells after treatment with MβCDX (1% for 15 min), indicating DISC formation in SCC61 cells, whereas in SQ20B cells, no DISC formation was observed (Fig. 7A). As a control, no modification of Fas expression in SQ20B or SCC61 cell lysates was observed (Fig. 7B), which rules out any over-expression of this receptor after MβCDX treatment.

3.5. *Cholesterol depletion activates the epidermal growth factor receptor (EGFR) survival signaling pathway in SQ20B cells*

To better understand the difference of response of MβCDX treatment between SQ20B and SCC61 cells, we investigated the EGFR survival-signaling pathway, which has been previously described to be potentially activated independently of the presence of EGF [39]. Before elucidating whether or not EGFR clusters in the membranes of cholesterol-depleted cells contained activated receptors, we first observed that EGFR was overexpressed in SQ20B cells compared with SCC61 cells even in the absence of treatment with MβCDX (Fig. 8A). To determine whether cholesterol depletion in SQ20B cells contributed to the EGFR auto-phosphorylation, we made use of a specific antibody raised against a phosphorylated form of EGFR (phosphorylation on Tyr-1173) since the phosphorylation of this site by Src kinases was previously reported to be characteristic of an activated form of EGFR [40]. As shown in Fig. 8B, treatment of SQ20B cells with 2% MβCDX for 1 h was associated with an increase in EGF-stimulated receptor autophosphorylation. By contrast, no phosphorylation of EGFR was observed in SCC61 cells after cholesterol depletion with MβCDX (data not shown). This result was confirmed with fluorescent microscopy imaging (Fig. 8C), which showed a significant increase of fluorescence in SQ20B cells after treatment with MβCDX, compared to untreated cells, corresponding to the phosphorylated EGFR. As expected, no fluorescence was observed in SCC61 cells regardless of the incubation time and the concentration of MβCDX used (Fig. 8C).

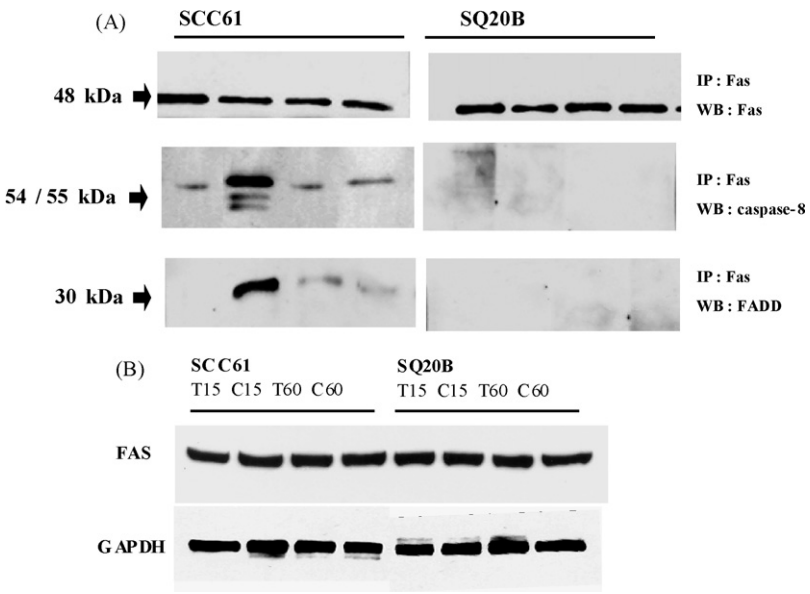

Fig. 7 – Activation of Fas and formation of Fas–FADD complexes in SCC61 cells after cholesterol depletion by MβCDX. Panel A: serum-starved SCC61 and SQ20B cells were preincubated with or without 1% MβCDX for 15 or 60 min at 37 °C and lysed with RIPA buffer. Lysates (300 μg) were immunoprecipitated with anti-Fas antibody coupled to agarose, before being denaturated and analyzed by SDS-polyacrylamide gel electrophoresis. Proteins were transferred to nitrocellulose and analyzed by Western blotting with anti-Fas (as control), anti-FADD and anti-caspase-8 antibodies. As a control, the expression of Fas was analyzed (Panel B) in SCC61 and SQ20B cells after treatment with MβCDX. Thirty micrograms of cell lysates was subjected to SDS-PAGE and immunoblotted using anti-Fas and anti-GAPDH (loading control) antibodies.

4. Discussion

Cyclodextrins such as MβCDX can reversibly remove cholesterol from the plasma membrane [17,41]. This property has made MβCDX an agent that is used extensively to study the function of rafts which are membrane microdomains whose integrity and structure mainly depend on the presence of a high concentration of cholesterol. Our previous results have shown that γ-radiation results in a rearrangement of the plasma membrane rafts and signaling platforms in the radiosensitive squamous cell carcinoma line SCC61, leading to radiation-induced apoptosis. This reorganization was found to be defective in the radioresistant counterpart cell line, SQ20B [32]. In this study, we observed that the cholesterol content of lipid rafts in SQ20B is twice as high as that in SCC61 cells, a result that could at least partially explain this defective reorganization at the plasma membrane level. Subsequently, we observed that cholesterol depletion induced by MβCDX treatment resulted in a striking effect on the viability of SCC61 cells and to a lesser extend of SQ20B cells. MβCDX treatment resulted in the triggering of apoptosis in the SCC61 cell line that was augmented by γ-radiation. Cell death was mediated through the intrinsic apoptotic pathway involving mitochondria as evidenced by both a decrease in the mitochondrial membrane potential and the production of ROS. By contrast, whatever the concentration or the time of incubation with MβCDX used in this work, either alone or in combination with γ-radiation, we were not able to detect apoptosis in SQ20B cells.

Giving further insight into the cellular mechanism leading to apoptosis in SCC61 cells, our data demonstrate that apoptosis of these cells is associated with the cleavage of procaspase 8, the clustering of Fas the DISC formation. This unexpected finding contrasts with previous data on lymphoid cells, where MβCDX was found to inhibit rather than stimulate apoptosis [22,42,43], but is in accordance with results previously reported in a model of HaCaT keratinocytes [21,44]. In SCC61 cells, as in HaCaT keratinocytes [21], depletion of cholesterol with MβCDX treatment resulted in the initiation of a ligand-independent Fas clustering and DISC formation, leading to the cleavage of procaspase 8 and apoptosis. Our working hypothesis to explain these observations was that disruption of SCC61 cell rafts with MβCDX leads to a redistribution of Fas receptors, a fundamental regulatory event during the activation step of this death receptor leading to apoptosis.

As SQ20B cells remained resistant to MβCDX-triggered apoptosis as evidenced by the absence of cleavage of procaspase 8 and DISC formation, we investigated whether or not survival pathways could be involved in the resistance to death receptor-induced apoptosis [45,46]. Among these, activation of the EGFR signaling pathway in the absence of exogenously added ligand has been already been found to occur in some cellular systems. Recent reports showed that cholesterol might directly modulate EGFR kinase activity, as incubation with water-soluble cholesterol caused a decrease of EGFR tyrosine phosphorylation, suggesting that the presence of cholesterol negatively regulates EGFR kinase activity [47]. In the same way, cholesterol depletion was shown to increase the intrinsic tyrosine kinase activity of the EGFR in membranes generated from MβCDX-treated NIH 3T3 cells [39].

In our preliminary studies, we observed a strikingly high expression of EGF receptors in SQ20B cells when compared with SCC61 cells. Moreover, we observed that cholesterol

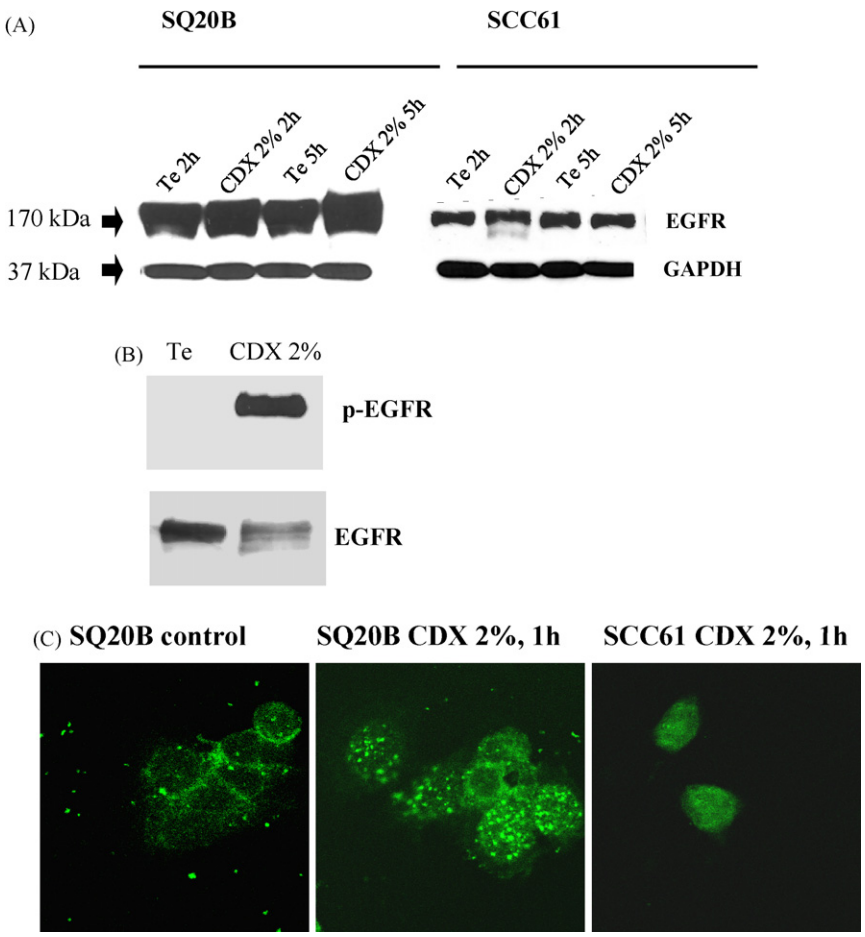

Fig. 8 – EGFR phosphorylation induced by MβCDX is ligand independent. Serum-starved SCC61 and SQ20B cells were pretreated with MβCDX (2% for 2 or 5 h) at 37 °C. After cell lysis, 20 μg of proteins was subjected to SDS-PAGE followed by Western blotting using specific anti-EGFR, anti-GAPDH (loading control) (Panel A) and anti-EGFR-P (Tyr-1173) (Panel B) antibodies. Panel C: serum-starved cells were treated as previously described, fixed with PFA and subjected to confocal microscopy analysis with EGFR-P (Tyr-1173) coupled to FITC antibodies.

depletion leads to an increase of EGF receptor phosphorylation of SQ20B cells in response to cholesterol depletion, a phenomenon that was not observed in SCC61 cells. This phosphorylation could be due to either an increase of the intrinsic kinase activity of the receptor or to a decrease in the rate of receptor dephosphorylation [39,47,48]. Tyrosines 992, 1045, 1068 and 1173 are all known sites of EGF receptor autophosphorylation [49,50]: the phosphorylation of tyrosines 992 and 1173 was routinely enhanced 1.5–2-fold following cholesterol depletion, whereas tyrosines 1045 and 1068 were minimally affected. Additionally, cholesterol depletion is followed by the disruption of lipid rafts and the loss of the EGF receptor from this compartment [39,51]. Because cholesterol is critical for inducing the formation of lipid rafts and because EGF receptors are normally localized within rafts, it is therefore tempting to speculate that the intracellular domain of the EGF receptor may adopt a different conformation when it is localized within rafts. This would give rise to differences in the accessibility of the various autophosphorylation sites and that would be reflected in the overall pattern of receptor phosphorylation [40].

Recent studies reported that cholesterol depletion by MβCDX induced ERK activation via the PI3K-dependent pathway [52] and tyrosine phosphorylation of multiple proteins such as EGFR and its downstream targets, including SHC, PLC-γ and Gab-1, as well as Ras activation [48]. Thus, it should be interesting to investigate in the near future the crosstalk in SQ20B cells between nonreceptor tyrosine kinases (as central transducers of the proliferative response) and caspases in order to check whether these two families of proteins can modulate each other's function through their enzymatic activities. Among the possibilities to explain the resistance to MβCDX-induced apoptosis of SQ20B cells, we can hypothesize that caspase-8 might be deactivated by phosphorylation as previously described in Jurkat and HeLa cells by Cursi et al. [53]. The Src family of nonreceptor tyrosine kinases is known to play an important role in the transduction of the proliferative signals triggered by growth factors such as PDGF, EGF or HGF [54]. Cursi et al. [53] showed that caspase-8 is phosphorylated on Tyr 380 not only in EGF receptor stimulation and EGF-impaired Fas-induced apoptosis, but also when Src kinase activity is pathologically upregulated such as in

colon cancer. This highlights Tyr 380 phosphorylation as a potential molecular strategy of apoptosis suppression adopted by tumor cells. In the same way, Alvarado-Kristensson et al. [55] showed that p38-MAPK could directly phosphorylate caspase-8 and caspase-3 on serine-364 and serine-150, respectively, inhibiting their activities and thereby hindering neutrophil apoptosis.

All these data support the idea that impairment of caspase-8 function may contribute to cancer development [56–58]. All the strategies targeting caspase-8 activation [59] and/or inhibition of Src kinases [60] should therefore be useful tools in order to sensitize human cancer cells to both chemo- and radiotherapy.

Acknowledgements

This work was supported by grants from the French ETOILE project of hadrontherapy and the the Ligue contre le Cancer, section de l'Ain. We thank the department of Immunology (Pr Bienvenu) of the Hospices Civils of Lyon, France.

REFERENCES

[1] Brown DA, London E. Functions of lipid rafts in biological membranes. Annu Rev Cell Dev Biol 1998;14:111–36.
[2] Burger K, Gimpl G, Fahrenholz F. Regulation of receptor function by cholesterol. Cell Mol Life Sci 2000;57:1577–92.
[3] Simons K, Toomre D. Lipid rafts and signal transduction. Nat Rev Mol Cell Biol 2000;1(1):31–9.
[4] Edidin M. The state of lipid rafts: from model membranes to cells. Annu Rev Biophys Biomol Struct 2003;32:257–83.
[5] Brown DA, London E. Structure and origin of ordered lipid domains in biological membranes. J Membr Biol 1998;164:103–14.
[6] Dobrowsky RT. Sphingolipid signalling domains floating on rafts or buried in caves? Cell Signal 2000;12:81–90.
[7] Dykstra M, Cherukuri A, Sohn HW, Tzeng SJ, Pierce SK. Location is everything: lipid rafts and immune cell signaling. Annu Rev Immunol 2003;21:457–81.
[8] Horejsi V. The roles of membrane microdomains (rafts) in T cell activation. Immunol Rev 2003;191:148–64.
[9] Pike LJ. Lipid rafts: bringing order to chaos. J Lipid Res 2003;44:655–67.
[10] Fielding CJ, Fielding PE. Membrane cholesterol and the regulation of signal transduction. Biochem Soc Trans 2004;32:65–9.
[11] Bollinger CR, Teichgraber V, Gulbins E. Ceramide-enriched membrane domains. Biochim Biophys Acta 2005;1746:284–94.
[12] Grassme H, Schwarz H, Gulbins E. Molecular mechanisms of ceramide-mediated CD95 clustering. Biochem Biophys Res Commun 2001;284:1016–30.
[13] Grassme H, Jekle A, Riehle A, Schwarz H, Berger J, Sandhoff K, et al. CD95 signaling via ceramide-rich membrane rafts. J Biol Chem 2001;276:20589–96.
[14] Lacour S, Hammann A, Grazide S, Lagadic-Gossmann D, Athias A, Sergent O, et al. Cisplatin-induced CD95 redistribution into membrane lipid rafts of HT29 human colon cancer cells. Cancer Res 2004;64:3593–8.
[15] Pike LJ. Growth factor receptors, lipid rafts and caveolae: an evolving story. Biochim Biophys Acta 2005;1746:260–73.
[16] Kabouridis PS, Janzen J, Magee AL, Ley SC. Cholesterol depletion disrupts lipid rafts and modulates the activity of multiple signaling pathways in T lymphocytes. Eur J Immunol 2000;30:954–63.
[17] Parpal S, Karlsson M, Thorn H, Stralfors P. Cholesterol depletion disrupts caveolae and insulin receptor signaling for metabolic control via insulin receptor substrate-1, but not for mitogen-activated protein kinase control. J Biol Chem 2001;276:9670–8.
[18] Yancey PG, Rodrigueza WV, Kilsdonk EP, Stoudt GW, Johnson WJ, Phillips MC, et al. Cellular cholesterol efflux mediated by cyclodextrins. Demonstration Of kinetic pools and mechanism of efflux. J Biol Chem 1996;271:16026–34.
[19] Hooper NM. Detergent-insoluble glycosphingolipid/cholesterol-rich membrane domains, lipid rafts and caveolae. Mol Membr Biol 1999;16:145–56.
[20] Ostermeyer AG, Beckrich BT, Ivarson KA, Grove KE, Brown DA. Glycosphingolipids are not essential for formation of detergent-resistant membrane rafts in melanoma cells. Methyl-beta-cyclodextrin does not affect cell surface transport of a GPI-anchored protein. J Biol Chem 1999;274:34459–66.
[21] Gniadecki R. Depletion of membrane cholesterol causes ligand-independent activation of Fas and apoptosis. Biochem Biophys Res Commun 2004;320:165–9.
[22] Hueber AO, Bernard AM, Herincs Z, Couzinet A, He HT. An essential role for membrane rafts in the initiation of Fas/CD95-triggered cell death in mouse thymocytes. EMBO Rep 2002;3:190–6.
[23] Mu Y, Lv S, Ren X, Jin G, Liu J, Yan G, et al. UV-B induced keratinocyte apoptosis is blocked by 2-selenium-bridged beta-cyclodextrin, a GPX mimic. J Photochem Photobiol B 2003;69:7–12.
[24] Algeciras-Schimnich A, Shen L, Barnhart BC, Murmann AE, Burkhardt JK, Peter ME. Molecular ordering of the initial signaling events of CD95. Mol Cell Biol 2002;22:207–20.
[25] Scheel-Toellner D, Wang K, Singh R, Majeed S, Raza K, Curnow SJ, et al. The death-inducing signalling complex is recruited to lipid rafts in Fas-induced apoptosis. Biochem Biophys Res Commun 2002;297:876–9.
[26] Gajate C, Mollinedo F. The antitumor ether lipid ET-18-OCH(3) induces apoptosis through translocation and capping of Fas/CD95 into membrane rafts in human leukemic cells. Blood 2001;98:3860–3.
[27] van der Luit AH, Budde M, Ruurs P, Verheij M, van Blitterswijk WJ. Alkyl-lysophospholipid accumulates in lipid rafts and induces apoptosis via raft-dependent endocytosis and inhibition of phosphatidylcholine synthesis. J Biol Chem 2002;277:39541–7.
[28] Hossain K, Akhand AA, Kawamoto Y, Du J, Takeda K, Wu J, et al. Caspase activation is accelerated by the inhibition of arsenite-induced, membrane rafts-dependent Akt activation. Free Radic Biol Med 2003;34:598–606.
[29] Li HY, Appelbaum FR, Willman CL, Zager RA, Banker DE. Cholesterol-modulating agents kill acute myeloid leukemia cells and sensitize them to therapeutics by blocking adaptive cholesterol responses. Blood 2003;101:3628–34.
[30] Rodriguez-Lafrasse C, Alphonse G, Aloy MT, Ardail D, Gerard JP, Louisot P, et al. Increasing endogenous ceramide using inhibitors of sphingolipid metabolism maximizes ionizing radiation-induced mitochondrial injury and apoptotic cell killing. Int J Cancer 2002;101:589–98.
[31] Alphonse G, Aloy MT, Broquet P, Gerard JP, Louisot P, Rousson R, et al. Ceramide induces activation of the mitochondrial/caspases pathway in Jurkat and SCC61 cells sensitive to gamma-radiation but activation of this sequence is defective in radioresistant SQ20B cells. Int J Radiat Biol 2002;78:821–35.

[32] Bionda C, Hadchity E, Alphonse G, Chapet O, Rousson R, Rodriguez-Lafrasse C, et al. Radioresistance of human carcinoma cells is correlated to a defect in raft membrane clustering. Free Radic Biol Med 2007;43:681–94.
[33] Gimpl G, Burger K, Fahrenholz F. Cholesterol as modulator of receptor function. Biochemistry 1997;36:10959–74.
[34] Gery B, Coppey J, Little JB. Modulation of clonogenicity, growth, and radiosensitivity of three human epidermoid tumor cell lines by a fibroblastic environment. Int J Radiat Oncol Biol Phys 1996;34:1061–71.
[35] Lisanti MP, Tang Z, Scherer PE, Sargiacomo M. Caveolae purification and glycosylphosphatidylinositol-linked protein sorting in polarized epithelia. Methods Enzymol 1995;250:655–68.
[36] Becart J, Chevalier C, Biesse J. Quantitative analysis of phospholipids by HPLC with a light-scattering evaporating detector—application to raw materials for cosmetic use. J High Resolut Chromatogr 1990;13:126–9.
[37] Gambert P, Lallemant C, Archambault A, Maume BF, Padieu P. Assessment of serum cholesterol by two methods: gas–liquid chromatography on a capillary column and chemical ionization-mass fragmentography with isotopic dilution of [3,4-13C] cholesterol as internal standard. J Chromatogr 1979;162:1–6.
[38] Gamble W, Vaughan M, Kruth HS, Avigan J. Procedure for determination of free and total cholesterol in micro- or nanogram amounts suitable for studies with cultured cells. J Lipid Res 1978;19:1068–70.
[39] Pike LJ, Casey L. Cholesterol levels modulate EGF receptor-mediated signaling by altering receptor function and trafficking. Biochemistry 2002;41:10315–22.
[40] Westover EJ, Covey DF, Brockman HL, Brown RE, Pike LJ. Cholesterol depletion results in site-specific increases in epidermal growth factor receptor phosphorylation due to membrane level effects. Studies with cholesterol enantiomers. J Biol Chem 2003;278:51125–33.
[41] Hao M, Mukherjee S, Maxfield FR. Cholesterol depletion induces large scale domain segregation in living cell membranes. Proc Natl Acad Sci USA 2001;98:13072–7.
[42] Muppidi JR, Siegel RM. Ligand-independent redistribution of Fas (CD95) into lipid rafts mediates clonotypic T cell death. Nat Immunol 2004;5(2):182–9.
[43] Garofalo T, Misasi R, Mattei V, Giammarioli AM, Malorni W, Pontieri GM, et al. Association of the death-inducing signaling complex with microdomains after triggering through CD95/Fas. Evidence for caspase-8-ganglioside interaction in T cells. J Biol Chem 2003;278:8309–15.
[44] Schonfelder U, Radestock A, Elsner P, Hipler UC. Cyclodextrin-induced apoptosis in human keratinocytes is caspase-8 dependent and accompanied by mitochondrial cytochrome c release. Exp Dermatol 2006;15:883–90.
[45] Nicholson DW. From bench to clinic with apoptosis-based therapeutic agents. Nature 2000;407:810–6.
[46] Igney FH, Krammer PH. Death and anti-death: tumour resistance to apoptosis. Nat Rev Cancer 2002;2:277–88.
[47] Ringerike T, Blystad FD, Levy FO, Madshus IH, Stang E. Cholesterol is important in control of EGF receptor kinase activity but EGF receptors are not concentrated in caveolae. J Cell Sci 2002;115:1331–40.
[48] Chen X, Resh MD. Cholesterol depletion from the plasma membrane triggers ligand-independent activation of the epidermal growth factor receptor. J Biol Chem 2002;277:49631–7.
[49] Hsuan JJ, Totty N, Waterfield MD. Identification of a novel autophosphorylation site (P4) on the epidermal growth factor receptor. Biochem J 1989;262(2):659–63.
[50] Downward J, Parker P, Waterfield MD. Autophosphorylation sites on the epidermal growth factor receptor. Nature 1984;311:483–5.
[51] Pike LJ, Miller JM. Cholesterol depletion delocalizes phosphatidylinositol bisphosphate and inhibits hormone-stimulated phosphatidylinositol turnover. J Biol Chem 1998;273:22298–304.
[52] Chen X, Resh MD. Activation of mitogen-activated protein kinase by membrane-targeted Raf chimeras is independent of raft localization. J Biol Chem 2001;276:34617–23.
[53] Cursi S, Rufini A, Stagni V, Condo I, Matafora V, Bachi A, et al. Src kinase phosphorylates caspase-8 on Tyr380: a novel mechanism of apoptosis suppression. EMBO J 2006;25:1895–905.
[54] Bromann PA, Korkaya H, Courtneidge SA. The interplay between Src family kinases and receptor tyrosine kinases. Oncogene 2004;23:7957–68.
[55] Alvarado-Kristensson M, Melander F, Leandersson K, Ronnstrand L, Wernstedt C, Andersson T. p38-MAPK signals survival by phosphorylation of caspase-8 and caspase-3 in human neutrophils. J Exp Med 2004;199:449–58.
[56] Teitz T, Wei T, Valentine MB, Vanin EF, Grenet J, Valentine VA, et al. Caspase 8 is deleted or silenced preferentially in childhood neuroblastomas with amplification of MYCN. Nat Med 2000;6:529–35.
[57] Kim HS, Lee JW, Soung YH, Park WS, Kim SY, Lee JH, et al. Inactivating mutations of caspase-8 gene in colorectal carcinomas. Gastroenterology 2003;125:708–15.
[58] Ashley DM, Riffkin CD, Muscat AM, Knight MJ, Kaye AH, Novak U, et al. Caspase 8 is absent or low in many ex vivo gliomas. Cancer 2005;104:1487–96.
[59] Ganten TM, Haas TL, Sykora J, Stahl H, Sprick MR, Fas SC, et al. Enhanced caspase-8 recruitment to and activation at the DISC is critical for sensitisation of human hepatocellular carcinoma cells to TRAIL-induced apoptosis by chemotherapeutic drugs. Cell Death Differ 2004;(Suppl. 1):S86–96.
[60] Griffiths GJ, Koh MY, Brunton VG, Cawthorne C, Reeves NA, Greaves M, et al. Expression of kinase-defective mutants of c-Src in human metastatic colon cancer cells decreases Bcl-xL and increases oxaliplatin- and Fas-induced apoptosis. J Biol Chem 2004;279:46113–21.